NANO LETTERS

pubs.acs.org/NanoLett

$LiMnPO_4$ Nanoplate Grown via Solid-State Reaction in Molten Hydrocarbon for Li-Ion Battery Cathode

Daiwon Choi,*,† Donghai Wang,†,§ In-Tae Bae,‡ Jie Xiao,† Zimin Nie,† Wei Wang,† Vilayanur V. Viswanathan,† Yun Jung Lee,† Ji-Guang Zhang,† Gordon L. Graff,† Zhenguo Yang,† and Jun Liu†

†Pacific Northwest National Laboratory, 902 Battelle Boulevard P.O. Box 999, Richland, Washington 99352 and ‡Small Scale Systems Integration and Packaging Center, State University of New York at Binghamton, P.O. Box 6000, Binghamton, NY 13902

ABSTRACT Electrochemically active $LiMnPO_4$ nanoplates have been synthesized via a novel, single-step, solid-state reaction in molten hydrocarbon. The olivine-structured $LiMnPO_4$ nanoplates with a thickness of ~50 nm appear porous and were formed as nanocrystals were assembled and grew into nanorods along the [010] direction in the (100) plane. After carbon coating, the prepared $LiMnPO_4$ cathode demonstrated a flat potential at 4.1 V versus Li with a specific capacity reaching as high as 168 mAh/g under a galvanostatic charging/discharging mode, along with an excellent cyclability.

KEYWORDS Li-ion battery, cathode, $LiMnPO_4$, surfactant, nanoplate

Recently, increasing demands for a clean environment and sustainable energy sources have stimulated significant effort in developing rechargeable Li-ion batteries, considered to be one of the most promising energy storage systems. Consequently, a strong research effort has focused on developing cheaper, safer, more stable, higher energy, and higher power Li-ion batteries to replace the conventional $LiCoO_2$, $LiNiO_2$, $LiMn_2O_4$, and graphite-based battery cells.[1−21] Following the initial work by Padhi et al. on the inductive effects of polyanions in a phospho-olivine $LiFePO_4$ cathode with an increased $Fe^{2+/3+}$ redox couple potential, olivine structures have become the focus of Li-ion battery cathodes in recent years.[2,3] Furthermore, the major obstacles encountered in using low ionic/electronic conductive $LiFePO_4$ cathodes have been overcome. Nanotechnology has made it possible to control particle size and apply electrically conductive coatings, and the process has now been optimized for high-power applications that are commercially available.[4,5]

Encouraged by the success of $LiFePO_4$, much research is now focused on the more challenging olivine $LiMPO_4$ (M = Mn, Co, and Ni) structures, especially $LiMnPO_4$ with a higher theoretical energy density (701 Wh/kg = 171 mAh/g × 4.1 V) due to higher potential than that of $LiFePO_4$ (586Wh/kg = 170 mAh/g × 3.45 V), which is considered as the maximum energy density practically achievable within the stability window of well-known carbonate ester-based electrolytes.[3,6] The other members of the olivine family, $LiCoPO_4$ and $LiNiPO_4$, are more challenging in the effort to develop stable electrolytes because of their higher voltage (4.8 and 5.1 V) vs Li/Li^+.[7] However, along with low ionic conductivity, the electronic conductivity of $LiMnPO_4$ ($<10^{-10}$ Scm^{-1}) is much lower than that of $LiFePO_4$ ($1.8 \times 10^{-9}Scm^{-1}$ at 25 °C), rendering it difficult to obtain decent electrochemical activity.[7,22] Additionally, possible key rate limiting factors, such as passivation phenomenon upon delithiation, Jahn−Teller anisotropic lattice distortion in Mn^{3+}, interface strain due to the large volume change between $LiMnPO_4$ and $MnPO_4$, and the metastable nature of the delithiated $MnPO_4$ phase, were suggested causes and are still under debate.[8] Tremendous effort has been made in recent years to overcome these limitations by particle-size minimization, substitutional doping, and enhancement of electronic contact between particles.[1,3,6−21,23−25] Thereby, various methods have been used to synthesize phase-pure nanosized $LiMnPO_4$, including precipitation, hydrothermal, sol−gel, polyol and solid state in highly porous carbon composites.[1,3,6−21,23−25] However, to date only few groups were able to attain more than 120 mAh/g from $LiMnPO_4$ in contrast to an abundance of studies on $LiFePO_4$.[1,6,8,9,12,15,16,23,25] Especially, large polarization during charging has been significant problem for achieving reasonable rate. For Li-ion battery cathode materials, crystallinity is as important as particle size, but widely known nanomaterial synthesis methods are generally designed for low-temperature routes to avoid grain growth and agglomeration. Such low-temperature routes lead to Mn^{2+} disorder

* To whom correspondence should be addressed. E-mail: daiwon.choi@pnl.gov. Phone: 509-375-4341. Fax: 509-375-4448.

§ Present address: The Pennsylvania State University, Department of Mechanical and Nuclear Engineering, University Park, PA 16802.

Received for review: 02/27/2010
Published on Web: 07/19/2010

DOI: 10.1021/nl1007085 | *Nano Lett.* **2010,** *10,* 2799–2805

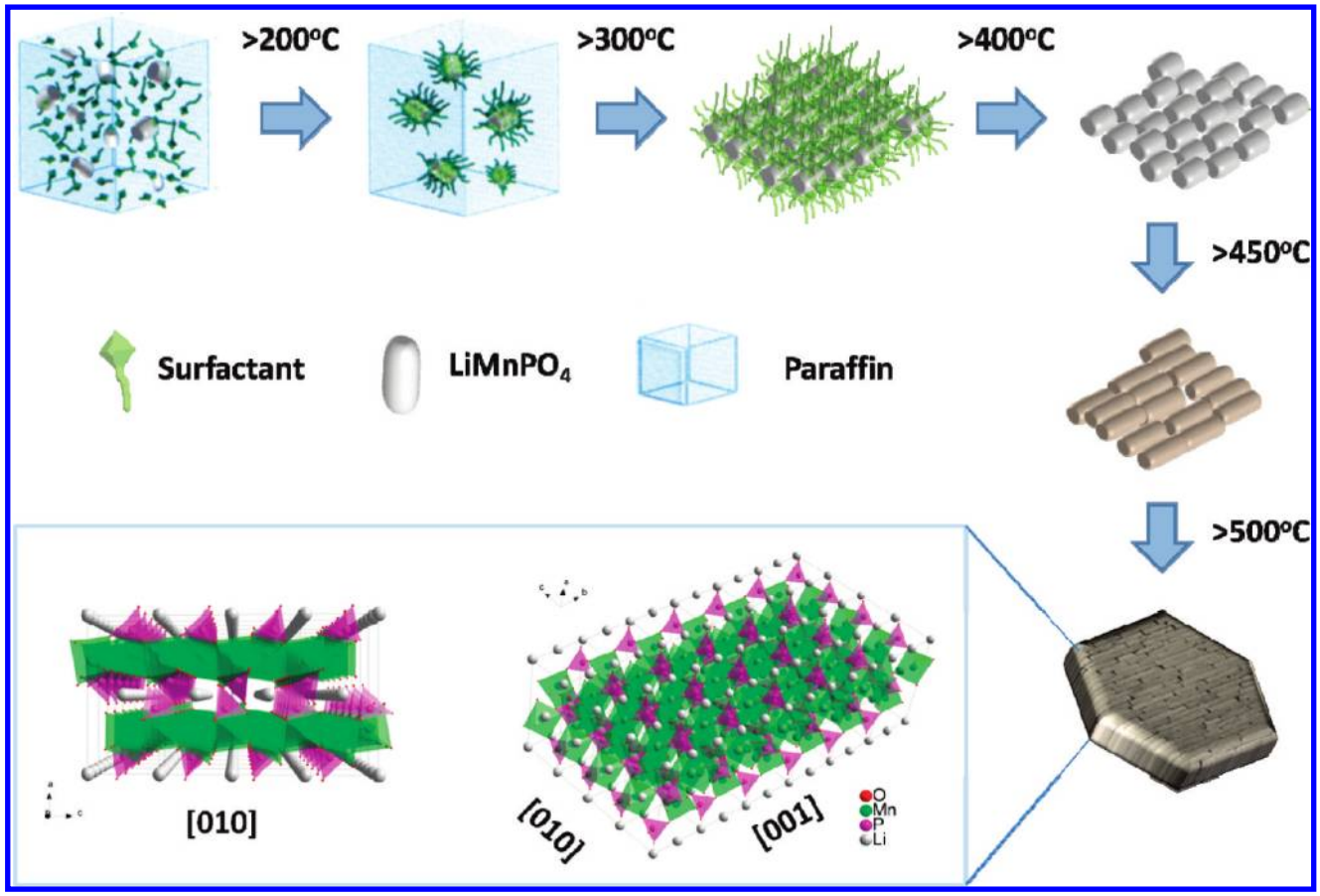

FIGURE 1. Schematic drawing of a molten hydrocarbon-assisted solid-state approach for making $LiMnPO_4$ nanoplates and their crystallographic orientation.

on the Li^+ sites in $LiMnPO_4$, which blocks the one-dimensional (1D) diffusion path of Li ions, thus limiting the electrochemical activity.[21,22] Additionally, high-potential cathode materials require a higher sintering temperature to form a more thermodynamically stable structure with stronger bonding. Simplicity of the synthesis process is vital for commercializing Li-ion batteries, and elaborate chemical routes are often less attractive in real-world applications. A solid-state reaction in molten surfactant-paraffin media using low-cost and green reagents that mimic both a solid-state and a self-assembly approach has been devised for $LiMnPO_4$ synthesis. Advantages of both routes have been combined into a single step to obtain well-dispersed uniform $LiMnPO_4$ nanoplates with good crystallinity and excellent electrochemical activity as a Li-ion battery cathode.

Figure 1 shows the molten hydrocarbon-assisted solid-state reaction for synthesizing uniform $LiMnPO_4$ nanoplates where oleic acid is used as a surfactant, and paraffin acts as a nonpolar solvent that facilitates thermodynamically preferred crystal growth of $LiMnPO_4$ without agglomeration. Surfactants are often oligomeric molecules involving two parts with different polarities: a high-polarity part that anchors to metal or oxide surfaces and a lower polar tail section that extends into the solvent, thereby maintaining its steric stability.[26−28] Such amphiphilic character of the molecule thus facilitates self-assembly to form nanocrystals with size and shape control.[26,27] The role of the oleic acid ($CH_3(CH_2)_7CH{=}CH(CH_2)_7COOH$), a monounsaturated omega-9 fatty acid found in various animal and vegetable sources, is to act as a surface-capping ligand of precursors with its carboxylic group and prevent agglomeration by steric hindrance during formation of the $LiMnPO_4$ nanocrystals.[23,28−35] A long alkyl chain of oleic acid coupled with −C═C− in the middle provides a better surface capping that dictates the shape of nanocrystals by thermodynamic means, making some crystallographic planes more favorable to grow by reducing their interfacial energies.[27] Consequently, the alkyl chain length can solely control the aspect ratio of the particles where an increase in the number of carbon atoms generally results in the formation of thinner but longer nanorods.[32] Additionally, oleic acid plays a substantial role in preventing the agglomeration of the particles. For oleic acid to form a uniform surface coating and extend its tail effectively, a well-matched solvent is required. Alkane hydrocarbons C_nH_{2n+2} ($20 \leq n \leq 40$), commonly known as paraffin, meaning "lacking reactivity" in Latin, are chemically inert because alkanes are nonpolar and lacking in functional groups. Under standard conditions, ($1 \leq n \leq 4$) alkanes are gaseous, ($5 \leq n \leq 17$) are liquids, and ($18 \leq n$) are solids called paraffin wax. As the boiling point of alkanes

DOI: 10.1021/nl1007085 | *Nano Lett.* **2010,** *10,* 2799--2805

is primarily determined by molecular weight and has an almost linear relationship with the size of the molecule, the boiling point rises approximately 20−30 °C for each carbon added to the chain. Pure colorless paraffin wax has a typical melting point between about 47 and 64 °C, and with a boiling point above 210 °C it is an excellent material to store heat (C_P: 2.1−2.9 J $g^{-1}K^{-1}$), it also expands considerably as it melts. Such paraffin wax can replace organic solvents used for low-temperature chemical synthesis. As a solvent and a surfactant, paraffin and oleic acid are cheap, environmentally friendly, and provide a stable environment for moisture-sensitive precursors because of their hydrophobic nature.[29]

All precursors used for $LiMnPO_4$ synthesis were analyzed with thermogravimetric analysis-differential thermal analysis (TGA-DTA) up to 650 °C under a 3 % H_2/97 % Ar atmosphere with a heating rate of 5 °C/min (Supporting Information, Figure S1). The precursor mixture after high-energy mechanical milling was heated in the tube furnace where precursors are dispersed by surfactants at <200 °C. The paraffin matrix enhances homogeneous oleic acid surface adsorption on $MnCO_3$. At temperatures between about 200 and 300 °C, excess oleic acid was removed, leaving only an oleic acid capping layer on the $MnCO_3$ surface. A slow evaporation of paraffin occurs over a broad temperature range between 210 and 350 °C because of a different molecular weight ($20 \leq n \leq 40$) in the mixture, which is ideal for matrix removal without affecting nucleation and crystallization of the $LiMnPO_4$ morphology. At 200 °C, $NH_4H_2PO_4$ melts, and pure $MnCO_3$ decomposes into MnO and CO_2, which is complete at 400 °C under 3 % H_2/97 % Ar atmosphere.[36,37] However, with the presence of $NH_4H_2PO_4$, $MnCO_3$ decomposes at a lower temperature (<250 °C) (Supporting Information, Figure S2). At this stage, the growth of $MnPO_4$ nanocrystals is believed to occur where phosphate anions compete with a surface-attached oleic acid layer, forming nanosized primary particles. They are self-assembled into the platelet morphology observed in $MnPO_4 \cdot xH_2O$.[19,20] As lithium acetate ($LiCOOCH_3$) melts at 286 °C, $LiMnPO_4$ crystallization finalizes at 350 °C (Supporting Information, Figures S2 and S3). The oleic acid plays a role as a surface-capping agent that protects the outer surface of the newly formed $LiMnPO_4$ nanocrystals, thus avoiding the possibility of further growth. Above 400°C, the decomposition of the surface-capped oleic acid ligand occurs where self-assembled $LiMnPO_4$ nanocrystals are further grown into nanorods and sintered in a preferred orientation without agglomeration of secondary particles, leading to $LiMnPO_4$ nanoplate morphology (Supporting Information, Figure S4). The crystallite size calculated from the XRD patterns at different stages of temperatures shows LiMnPO formation at 300−350°C, followed by negligible grain growth up to 450°C. Above 450°C, more rapid grain growth occurs up to 550°C where the final crystallite size was ∼25 nm (Supporting Information, Figure S3), which is believed to be caused by the growth of self-assembled $LiMnPO_4$ nanorods as the oleic acid surface capping layer is removed.

The role of surface oleic acid in nanoparticle synthesis has been reported previously for Co and Ni nanocrystals where thermal desorption of the surfactant was observed at 200 °C followed by dehydrogenation at 400 °C, leaving a graphitic surface with oleic acid fragmented into alkanes underneath. This was confirmed by near-edge X-ray absorption fine structure (NEXAFS) spectral signatures corresponding to the specific chemical configurations, such as the carboxylic acid group, the alkane backbone, and the graphitic carbon C=C π^* peak.[29,38] The final crystallization of $LiMnPO_4$ was done at 550 °C, leaving only <1.2 wt % final carbon residue.

Figure 2a,b,e shows FESEM images of uniformly dispersed $LiMnPO_4$ nanoplates synthesized via a molten hydrocarbon-assisted, solid-state reaction. The $LiMnPO_4$ nanoplate is approximately 50 nm in thickness and has an in-plane extension as long as 1−2 μm. There are few reports on $LiMnPO_4$ nanoplate synthesis using different approaches, but nanoplates tend to stack on top of each other, forming agglomerates.[16,19] The $LiMnPO_4$ nanoplates obtained by a solid-state reaction in molten hydrocarbon are well dispersed without stacking, and each nanoplate can be easily dispersed. HRTEM and FESEM analyses indicate that these $LiMnPO_4$ nanoplates constitute a porous structure formed by self-assembling nanorods aligned in a preferred orientation with a high specific surface area of 37.3 m^2/g measured with the BET technique. With a uniform conductive coating, such a porous structure would lead to reduced polarization, especially during the charging process where the galvanostatic−potentiostatic combination mode had to be used to fully charge $LiMnPO_4$ by the others.[1,9,12,20,23,25]

Figure 2d shows Rietveld refinement on the X-ray diffraction (XRD) pattern of the $LiMnPO_4$ nanoplates based on the orthorhombic *Pnma* space group where *b* and *a* axes were switched from *Pnmb* (JCPDS No. 33-0804), which is isostructural to $LiFePO_4$. The refined lattice parameter matches closely to that of pure orthorhombic $LiMnPO_4$ (*Pnma*, $a = 10.441(1)$, $b = 6.101(3)$, $c = 4.747(3)$ Å). The Li-ion diffusion pathway in the olivine $LiMPO_4$ (M: Fe or Mn) structure is known to be along the 1D [010] direction.[16,22,39]

To confirm the preferred growth, the crystallographic orientation of $LiMnPO_4$ nanoplates was analyzed with the nanobeam electron diffraction (NBED) technique (probe size ∼50 nm) by orienting the incident beam directly perpendicular to the nanoplates as shown in Figure 2h. The corresponding NBED pattern is shown in Figure 2g. The crystallographic orientation was compared to a simulated diffraction pattern shown in Figure 2f by calculating the structure factor, F_{hkl}, where *hkl* represents a specific Bragg reflection based on kinematical approximation. As a result, it was found that the NBED pattern corresponds to [100] of $LiMnPO_4$. Note that the forbidden Bragg reflections denoted by white arrows in Figure 2g are due to double diffraction.

DOI: 10.1021/nl1007085 | *Nano Lett.* **2010,** *10,* 2799--2805

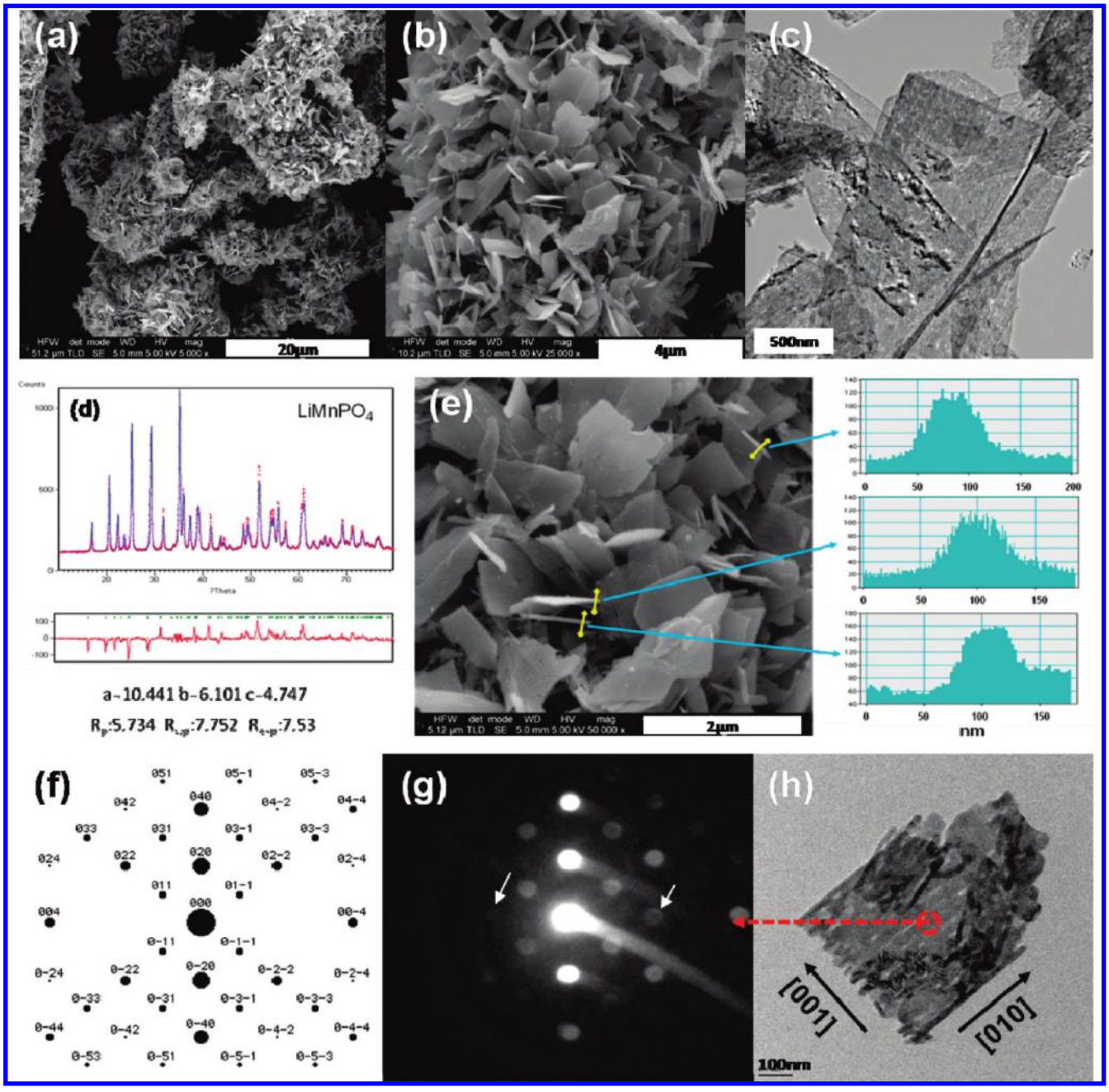

FIGURE 2. (a,b,e) Field emission scanning electron microscopy (FESEM) and (c,h) high-resolution transmission electron microscopy (HRTEM) images of $LiMnPO_4$ nanoplates, (d) Rietveld refinement of $LiMnPO_4$, (f) simulated diffraction pattern with incident electron beam parallel to [100], (g) nanobeam electron diffraction pattern, and (h) orientation of $LiMnPO_4$ grown via the molten hydrocarbon approach.

By examining several $LiMnPO_4$ nanoplates, we found that these $LiMnPO_4$ nanoplates show identical orientation with preferred growth on the order of [010] > [001] > [100] with [010] and [001] being very close. This coincides with that reported for $LiMPO_4$ (M: Fe or Mn).[19,40] There have been reports on $LiMnPO_4$ nanoplates with the shortest crystal orientation being [010].[16] However, our analyses show that the thinnest part of the nanoplate is along the *a*-axis [100], which is not a favorable direction for the Li ion diffusion. Nevertheless, the [010] growth is more favorable for a cathode material because a flat potential is guaranteed by the two-phase transition during the electrochemical Li insertion/extraction process. In the case of isostructural $LiFePO_4$, the crystal size around 40 nm shows a single-phase transformation during Li extraction/insertion at room temperature, giving a sloping voltage profile.[18,40] Consequently, the size of olivine structured particles being too small (<80 nm) cannot provide high-energy density.

To optimize $LiMnPO_4$ performance as a cathode, a carbon coating was applied to well-dispersed uniform $LiMnPO_4$ nanoplates. Planetary ball milling has been widely used for making the $LiMnPO_4$/C composite and is also a critical step

DOI: 10.1021/nl1007085 | *Nano Lett.* **2010,** *10,* 2799–2805

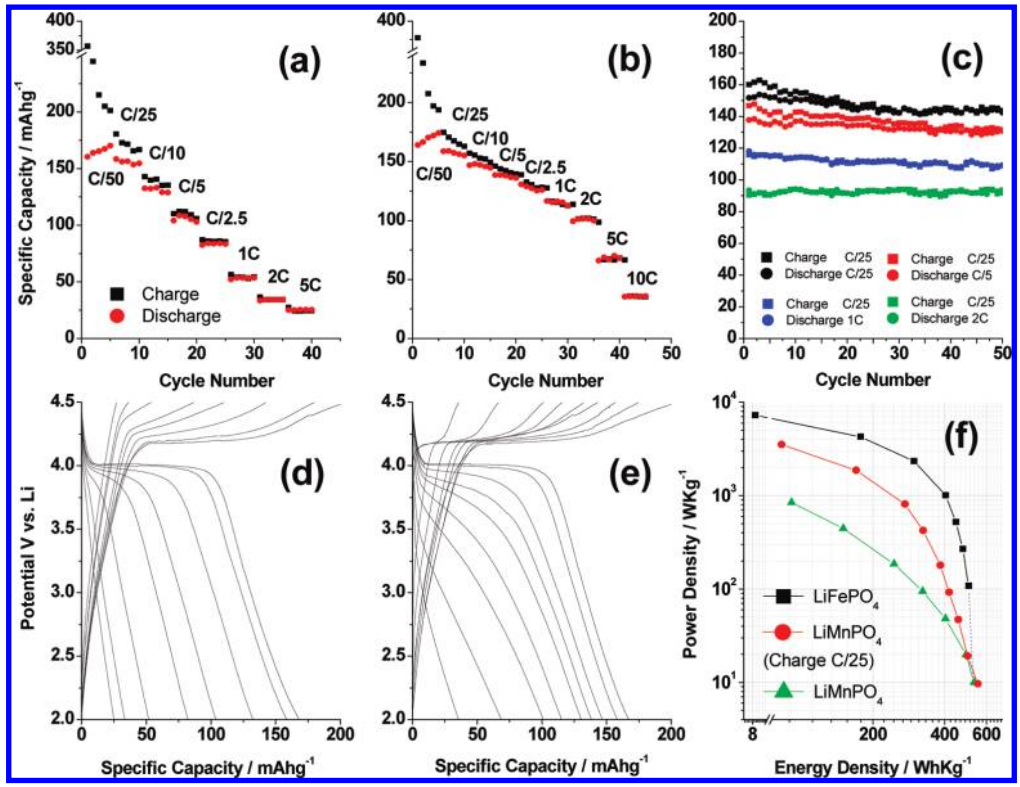

FIGURE 3. Rate performance of $LiMnPO_4$ during (a) same charge/discharge C-rates and (b) various discharge C-rates following constant charge at C/25 and (c) extended electrochemical cycling on cells after rate evaluations. Voltage-capacity profiles of $LiMnPO_4$ nanoplates cycled at (d) the same charge/discharge C-rates, (e) various discharge C-rates following constant charge at C/25, and f) Ragone plot comparison of $LiMnPO_4$ to $LiFePO_4$.

for maximizing electrochemical behavior from the given material morphology.[8,24,41] It should be noted that the milling process for carbon coating is sensitive to the material loading, rpm, time, number, and size of the balls used.[8,24,41] After ball milling with 20 wt % conductive carbon, larger $LiMnPO_4$/C secondary particles in the micrometer size range (Supporting Information, Figure S5) are obtained but with a higher specific surface area of 154.2 m^2/g. A slight decrease in crystallite size from 27.1 to 23.8 nm was observed, but no noticeable changes in the XRD pattern indicate no defect formation or changes in crystal structure after planetary milling (Supporting Information, Figure S6).[8,24,41] Additionally, the unique texture of the $LiMnPO_4$ nanoplate is maintained even after the balling milling process, as confirmed by the XRD analysis on the paper electrode made by rolling with polytetrafluoroethylene (PTFE) binder where milled $LiMnPO_4$ nanoplate powders were aligned in textured orientation (Supporting Information, Figure S6). Figure 3 shows the C-rate and cycling performance of the $LiMnPO_4$ nanoplate cathode at room temperature. Unlike many others using galvanostatic (constant current: CC)−potentiostatic (constant voltage: CV) combination mode charging followed by galvanostatic discharge, only the galvanostatic mode was used in our electrochemical evaluation. There were two different conditions for C-rate performance, one with increasing charge/discharge rates with the charge and discharge current being equal (Figure 3a,d) and the other with a constant charge rate that was followed by increasing discharge rates (Figure 3b,e). Such galvanostatic testing was possible because of comparatively lower polarization during the charging process.

Figure 3d,e presents typical voltage profiles of these $LiMnPO_4$/C cathodes at various discharge rates between C/50 and 10C, based on 150 mAh/g as a theoretical capacity. The voltage profiles clearly show a flat redox potential around 4.1 V versus Li/Li^+, indicating that the charge/discharge reaction proceeds via a first-order phase transition between $LiMnPO_4$ and $MnPO_4$. A specific capacity of 168 mAh/g was achieved at C/50, which is close to the theoretical capacity. At a 1C charge/discharge rate, a specific capacity of 54 mAh/g was delivered (Figure 3d), but 117 mAh/g was attained at the 1C discharge rate after charging at C/25 (Figure 3e). The rate performance comparison of $LiMnPO_4$ is difficult, especially because of the various conditions applied for the electrochemical evaluations. However, these results represent a significant advance over previous reports, which typically gave a much lower-than-theoretical reversible capacity, even at low charge/discharge rates. Furthermore, the $LiMnPO_4$ nanoplate cathode obtained does not require any secondary heat-treatment following carbon coating, additional carbon (>20 wt %), or a higher charging potential (>4.5 V).[9,25] For $LiMnPO_4$, other than lower electronic and ionic conductivities, the charging process limits the capacity because of a 3−4 times narrower potential window available

DOI: 10.1021/nl1007085 | *Nano Lett.* **2010,** *10,* 2799--2805

compared to the discharging process. On the other hand, $LiFePO_4$ has a more than twice as wide potential window for charging because of a lower Fe^{2+}/Fe^{3+} redox potential.

During the electrochemical cycling test, the initial charge showed almost twice as high specific capacity than the theoretical value, which stabilized upon prolonged cycles reaching columbic efficiency close to 100%. Similar behavior was observed by the others, and possible side reactions or passivation phenomena of the standard electrolyte solutions on the carbon part or the $LiMnPO_4$/C composite were proposed at high potentials.[20,23,25] Our preliminary analyses show that such an extended initial charge current is not related to the Al foil current collector and might be related to the carbon coating done by milling. Nevertheless, detailed initial irreversible loss phenomena on the $LiMnPO_4$/C composite cathode at high potentials need further exploration.

Figure 3f shows the Ragone plot of $LiFePO_4$ and $LiMnPO_4$ tested at a different mode where the power and energy density of $LiMnPO_4$ were normalized based on the active $LiFePO_4$ weight since $LiMnPO_4$ uses 20 wt % conductive carbon instead of 10 wt % in the $LiFePO_4$ cell, delivering a 12.5% reduction in energy/power densities. The $LiFePO_4$ tested for comparison was synthesized using the same solid-state reaction in the molten hydrocarbon approach with an $Fe(C_2O_4)_2 \cdot 2H_2O$ precursor.[42] Compared to $LiFePO_4$, $LiMnPO_4$ shows a lower rate performance due to lower electronic, ionic conductivity, and a larger difference between the surface and bulk potential, requiring higher activation energy to cross over the (010) plane.[22,39] However, the Ragone plot comparison indicates that the discharge power density of $LiMnPO_4$ is close to that of $LiFePO_4$ when fully charged at C/25, and the energy density of 551 Wh/kg (630 Wh/kg without normalization) is comparable to or higher than that of $LiFePO_4$ at lower power (<30 W/kg). The typical cycling behaviors of $LiMnPO_4$ in four different cells at various rates are presented in Figure 3c. In all experiments, the charge/discharge was carried out purely galvanostatically while charging was performed at the C/25 protocol. When using the voltage range of 2.0−4.5 V at room temperature, $LiMnPO_4$ shows stable cycling over 50 cycles without a noticeable fade in capacity, making $LiMnPO_4$ attractive as an alternative cathode material. However, further detailed studies are required for a $LiMnPO_4$ cathode, including stability of the delithiated $MnPO_4$ phase,[43,44] phase transition during the charging/discharging process, initial prolonged charging phenomena, electrolyte compatibility, and effective carbon coating to lower the carbon content, thereby increasing the energy density in the full cell.

Our $LiMnPO_4$ nanoplates obtained by a molten hydrocarbon-assisted, solid-state reaction can be easily scaled up for commercialization. This process shows potential for further improvement using a simplified synthesis route to obtain fully electrochemically active $LiMnPO_4$, which appears to be a promising cathode material for Li-ion batteries.

Acknowledgment. This work is supported by the Laboratory-Directed Research and Development Program of the Pacific Northwest National Laboratory (PNNL) and by the U.S. Department of Energy's (DOE's) Office of Energy Efficiency and Renewable Energy, Office of Electricity Delivery and Energy Reliability and Office of Vehicle Technologies. The transmission electron microscopy investigation was performed in the Environmental Molecular Sciences Laboratory, a national scientific user facility sponsored by DOE's Office of Biological and Environmental Research. PNNL is a multiprogram laboratory operated for DOE by Battelle under Contract DE-AC05-76RL01830. HRTEM support from Scale Systems Integration and Packaging (S^3IP) Center at SUNY Binghamton was provided by the Empire State Development Corporation.

Supporting Information Available. Experimental procedure and additional figures. This material is available free of charge via the Internet at http://pubs.acs.org.

REFERENCES AND NOTES

(1) Yonemura, M.; Yamada, A.; Takei, Y.; Sonoyama, N.; Kanno, R. *J. Electrochem. Soc.* **2004**, *151* (9), A1352–A1356.
(2) Padhi, A. K.; Najundaswamy, K. S.; Goodenough, J. B. *J. Electrochem. Soc.* **1997**, *144*, 1188–1194.
(3) Yamada, A.; Kudo, Y.; Liu, K.-Y. *J. Electrochem. Soc.* **2001**, *148* (7), A747–A754.
(4) Wang, Y.; Wang, Y.; Hosono, E.; Wang, K.; Zhou, H. *Angew. Chem., Int. Ed.* **2008**, *47*, 7461–7465.
(5) Choi, D.; Kumta, P. N. *J. Power Sources* **2007**, *163*, 1064–1069.
(6) Li, G.; Azuma, H.; Tohda, M. *J. Electrochem. Soc.* **2002**, *149* (6), A743–A747.
(7) Delacourt, C.; Laffont, L.; Bouchet, R.; Wurm, C.; Leriche, J.-B.; Morcrette, M.; Tarascon, J.-M.; Masqueliera, C. *J. Electrochem. Soc.* **2005**, *152* (5), A913–A921.
(8) Drezen, T.; Kwon, N.; Bowen, P.; Teerlinck, I.; Isono, M.; Exnar, I. *J. Power Sources* **2007**, *174*, 949–953.
(9) Shiratsuchi, T.; Okada, S.; Doi, T.; Yamaki, J. *Electrochim. Acta* **2009**, *54* (11), 3145–3151.
(10) Yamada, A.; Chung, S. *J. Electrochem. Soc.* **2001**, *148* (8), A960–A967.
(11) Chen, G.; Wilcox, J. D.; Richardson, T. J. *Electrochem. Solid-State Lett.* **2008**, *11* (11), A190–A194.
(12) Li, G.; Azuma, H.; Tohda, M. *Electrochem. Solid-State Lett.* **2002**, *5* (6), A135–A137.
(13) Yamada, A.; Hosoy, M.; Chung, S.-C.; Kudo, Y.; Hinokum, K.; Liu, K.-Y.; Nish, Y. *J. Power Sources* **2003**, *119−121*, 232–238.
(14) Fang, H.; Li, L.; Yang, Y.; Yan, G.; Li, G. *Chem. Commun.* **2008**, 1118–1120.
(15) Kwon, N.; Drezen, T.; Exnar, I.; Teerlinck, I.; Isono, M.; Graetzel, M. *Electrochem. Solid-State Lett.* **2006**, *9* (6), A277–A280.
(16) Wang, D.; Buqa, H.; Crouzet, M.; Deghenghi, G.; Drezen, T.; Exnar, I.; Kwon, N.; Miners, J. H.; Poletto, L.; Grätzel, M. *J. Power Sources* **2008**, *189* (1), 624–628.
(17) Delacourt, C.; Poizot, P.; Morcrette, M.; Tarascon, J.-M.; Masquelier, C. *Chem. Mater.* **2004**, *16*, 93–99.
(18) Kim, T. R.; Kim, D. H.; Ryu, H. W.; Moon, J. H.; Lee, J. H.; Boo, S.; Kim, J. *J. Phys. Chem. Solids* **2007**, *68*, 1203–1206.
(19) Bramnik, N. N.; Ehrenberg, H. *J. Alloys Compd.* **2008**, *464*, 259–264.
(20) Xiao, J.; Xu, W.; Choi, D.; Zhang, J.-G. *J. Electrochem. Soc.* **2010**, *157* (2), A142–A147.
(21) Fang, H.; Pan, Z.; Li, L.; Yang, Y.; Yan, G.; Li, G.; Wei, S. *Electrochem. Commun.* **2008**, *10*, 1071–1073.
(22) Morgan, A., D.; Van der Ven, A.; Ceder, G. *Electrochem. Solid-State Lett.* **2004**, *7* (2), A30–A32.
(23) Martha, S. K.; Markovsky, B.; Grinblat, J.; Gofer, Y.; Haik, O.; Zinigrad, E.; Aurbach, D.; Drezen, T.; Wang, D.; Deghenghi, G.; Exnar, I. *J. Electrochem. Soc.* **2009**, *156* (7), A541–A552.

DOI: 10.1021/nl1007085 | *Nano Lett.* **2010,** *10,* 2799–2805

(24) Doan, The N. L.; Bakenov, Z.; Taniguchi, I. *Adv. Powder Technol.* **2009**, *21* (2), 187–196.
(25) Bakenov, Z.; Taniguchi, I. *Electrochem. Commun.* **2010**, *12*, 75–78.
(26) Martha, S. K.; Grinblat, J.; Haik, O.; Zinigrad, E.; Drezen, T.; Miners, J. H.; Exnar, I.; Kay, A.; Markovsky, B.; Aurbach, D. *Angew. Chem., Int. Ed.* **2009**, *48*, 8559–8563.
(27) Xia, Y.; Xiong, Y.; Lim, B.; Skrabalak, S. E. *Angew. Chem., Int. Ed.* **2008**, *47*, 2–46.
(28) Chen, M.; Ding, W. H.; Kong, Y.; Diao, G. W. *Langmuir* **2008**, *24*, 3471–3478.
(29) Deng, Z.; Cao, L.; Tang, F.; Zou, B. *J. Phys. Chem. B* **2005**, *109*, 16671–16675.
(30) Khanna, P. K.; Kale, T. S.; Shaikh, M.; Koteswar Rao, N.; Satyanarayana, C. V. V. *Mater. Chem. Phys.* **2008**, *110*, 21–25.
(31) Liao, Y.-F.; Li, W.-J. *J. Zhejiang Univ., Sci., A* **2008**, *9* (1), 133–136.
(32) Dumestre, F.; Amiens, C.; Chaudret, B.; Fromen, M. C.; Casanove, M. J.; Renaud, P.; Zurcher, P. *Mater. Res. Soc. Symp. Proc.* , *735*, No. C10.4.1.
(33) Yu, W. W.; Falkner, J. C.; Yavuz, C. T.; Colvin, V. L. *Chem. Commun.* **2004**, *230*, 6–2307.
(34) Baoqing, S.; Jipeng, L.; Zhixue, W. *Chinese J. Chem. Eng.* **2006**, *14* (6), 814–818.
(35) Shao, H.; Huang, Y.; Lee, H. S.; Suha, Y. J.; Kim, C. O. *J. Appl. Phys.* **2006***99*, No. 08N702.
(36) Wang, D.; Li, H.; Wang, Z.; Wu, X.; Sun, Y.; Huang, X.; Chen, L. *J. Solid State Chem.* **2004**, *177*, 4582–4587.
(37) Shaheen, W. M.; Selim, M. M. *J. Therm. Anal. Calorim.* **2000**, *59*, 961–970.
(38) Perez-Dieste, V.; Castellini, O. M.; Crain, J. N.; Eriksson, M. A.; Kirakosian, A.; Lin, J.-L.; McChesney, J. L.; Himpsela, F. J. *Appl. Phys. Lett.* **2003**, *83* (24), 5053.
(39) Wang, L.; Zhou, F.; Ceder, G. *Electrochem. Solid-State Lett.* **2008**, *11* (6), A94–A96.
(40) Gibot, P.; Casas-Cabanas, M.; Laffont, L.; Levasseur, S.; Carlach, P.; Hamelet, S.; Tarascon, J.-M.; Masquelier, C. *Nat. Mater.* **2008**, *7*, 741–747.
(41) Rabanal, M. E.; Gutierrez, M. C.; Garcia-Alvarado, F.; Gonzalo, E. C.; Arroyo-de Dompablo, M. E. *J. Power Sources* **2006**, *160*, 523–528.
(42) Choi, D.; Wang, D.; Viswanathan, V. V.; Bae, I.-T.; Wang, W.; Nie, Z.; Zhang, J.-G.; Graff, G. L.; Liu, J.; Yang, Z.; Duong, T. *Electrochem. Commun.* **2010**, *12* (3), 427–430.
(43) Ong, S. P.; Jain, A.; Hautier, G.; Kang, B.; Ceder, G. *Electrochem. Commun.* **2010**, *12* (3), 378–381.
(44) Kim, S.-W.; Kim, J.; Gwon, H.; Kang, K. *J. Electrochem. Soc.* **2009**, *156* (8), A635–A638.

DOI: 10.1021/nl1007085 | *Nano Lett.* **2010,** *10,* 2799--2805